

# The crustal structure and tectonic development of the continental margin of the Amundsen Sea Embayment, West Antarctica: implications from geophysical data

Thomas Kalberg and Karsten Gohl

*Alfred Wegener Institute Helmholtz-Centre for Polar and Marine Research, Am Alten Hafen 26, D-27568 Bremerhaven, Germany.  
 E-mail: thomas.kalberg@awi.de*

Accepted 2014 March 26. Received 2014 March 25; in original form 2013 June 19

## SUMMARY

The Amundsen Sea Embayment of West Antarctica represents a key component in the tectonic history of Antarctic–New Zealand continental breakup. The region played a major role in the plate-kinematic development of the southern Pacific from the inferred collision of the Hikurangi Plateau with the Gondwana subduction margin at approximately 110–100 Ma to the evolution of the West Antarctic Rift System. However, little is known about the crustal architecture and the tectonic processes creating the embayment. During two ‘RV Polarstern’ expeditions in 2006 and 2010 a large geophysical data set was collected consisting of seismic-refraction and reflection data, ship-borne gravity and helicopter-borne magnetic measurements. Two *P*-wave velocity–depth models based on forward traveltimes modelling of nine ocean bottom hydrophone recordings provide an insight into the lithospheric structure beneath the Amundsen Sea Embayment. Seismic-reflection data image the sedimentary architecture and the top-of-basement. The seismic data provide constraints for 2-D gravity modelling, which supports and complements *P*-wave modelling. Our final model shows 10–14-km-thick stretched continental crust at the continental rise that thickens to as much as 28 km beneath the inner shelf. The homogenous crustal architecture of the continental rise, including horst and graben structures are interpreted as indicating that wide-mode rifting affected the entire region. We observe a high-velocity layer of variable thickness beneath the margin and related it, contrary to other ‘normal volcanic type margins’, to a proposed magma flow along the base of the crust from beneath eastern Marie Byrd Land—West Antarctica to the Marie Byrd Seamount province. Furthermore, we discuss the possibility of upper mantle serpentinization by seawater penetration at the Marie Byrd Seamount province. Hints of seaward-dipping reflectors indicate some degree of volcanism in the area after break-up. A set of gravity anomaly data indicate several phases of fully developed and failed rift systems, including a possible branch of the West Antarctic Rift System in the Amundsen Sea Embayment.

**Key words:** Submarine tectonics and volcanism; Tectonics and landscape evolution; Dynamics of lithosphere and mantle; Dynamics: gravity and tectonics; Antarctica.

## 1 INTRODUCTION

Studying the lithospheric architecture of the Amundsen Sea Embayment (ASE) of West Antarctica (Fig. 1) provides constraints on tectono-magmatic reconstructions of the West Antarctic continental margin and the embayment itself from Palaeozoic to Cenozoic times. Improved knowledge of the structure and development of the lithosphere is the key to unravelling the evolution of the West Antarctic continental margin and the corresponding landscapes. The area experienced a number of key events during the tectonic history of the southern Pacific, including the inferred collision of the Hikurangi Plateau with the Gondwana at approximately 110–

100 Ma subduction margin (Davy & Wood 1994; Mortimer *et al.* 2006) to the evolution of the West Antarctic Rift System. A number of plate-kinematic reconstructions are centred on the region, most recently by Eagles *et al.* (2004a) and Wobbe *et al.* (2012), but suffer from a lack of information about the deep crustal structure of the West Antarctic continental margin. The ASE also experienced a number of magmatic events from mid-Mesozoic to Late Cenozoic times (Wobbe *et al.* 2012). Analysis and modelling of magnetic data provides a first insight into the basement structure of the ASE shelf and implies that the present-day basement morphology of the ASE shelf may control the dynamic behaviour of grounded parts of the West Antarctic Ice Sheet (WAIS; Gohl 2012; Gohl *et al.* 2013a).

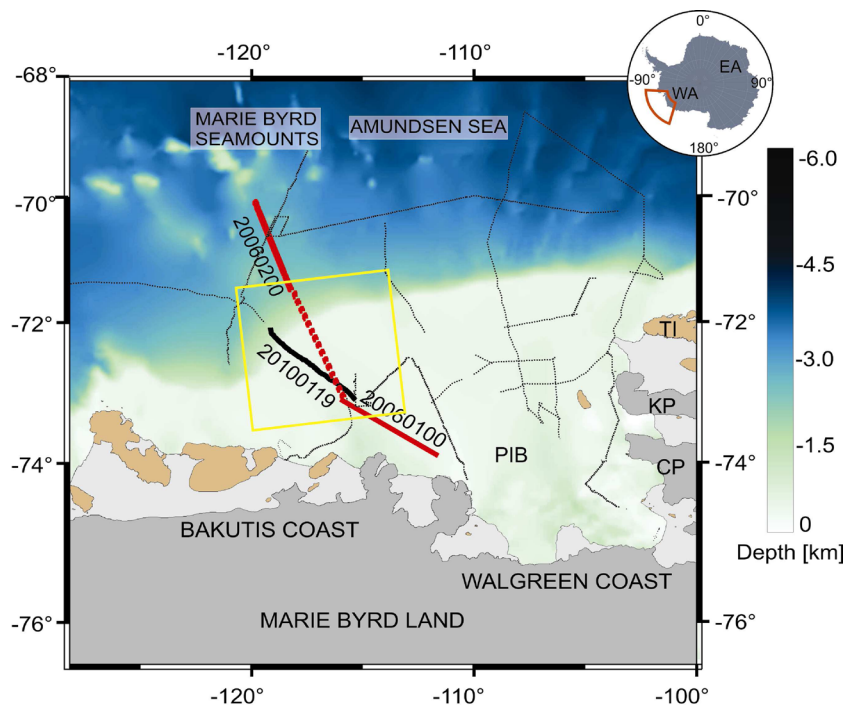


**Figure 1.** Bathymetric map of the Amundsen Sea Embayment after Nitsche *et al.* (2007) showing the locations of two OBH profiles and corresponding multichannel seismic reflection profiles (thick black lines). The red dashed line marks the interpolated profile AWI-100/200, connecting the profiles AWI-20060100 and AWI-20060200. Thin dotted black lines mark other seismic reflection profiles. The thin yellow frame shows the window which was used for the spectral analysis. TI, Thurston Island; PIB, Pine Island Bay; KP, King Peninsula; CP, Canisteo Peninsula.

An improved understanding of the tectono-magmatic processes and of the formation of basement ridges and sedimentary basins provides further constraints on palaeo and modern ice sheet dynamics as demonstrated in Bingham *et al.* (2012) or Smith *et al.* (2013).

This study presents a combination of geophysical data from the ASE, which were collected to study the lithospheric architecture and tectono-magmatic evolution of the West Antarctic continental margin. At first, we present and highlight the results of each individual data set. A continental rise-to-shelf seismic reflection transect provides constraints on the top-of-basement morphology and sedimentary architecture of the margin. Two deep crustal seismic refraction and wide-angle reflection profiles are used to derive velocity–depth profiles. Supported by a spectral analysis of gravity data, two different continuous 2-D forward gravity models place constraints on the crustal architecture and formation of the continental margin and shelf of the ASE. Following this, we propose a new integrated model of the tectonic evolution of the margin of the ASE. With this model we attempt to reconstruct the tectono-magmatic development of this margin from its breakup from New Zealand as early as 90 Ma (Wobbe *et al.* 2012) to the PRESENT which further supports boundary conditions for ice-sheet modelling attempts in this part of West Antarctica.

## 2 TECTONIC AND GEOLOGICAL BACKGROUND

The tectonic development of the Pacific margin of West Antarctica since Late Cretaceous times consisted of several distinct phases (Fig. 2). The southwestward propagation of rifting and breakup began with the separation of Chatham Rise from the Amundsen Sea margin of eastern Marie Byrd Land as early as 90 Ma and continued around 83 Ma with the breakup of Campbell Plateau from central

Marie Byrd Land (e.g. Mayes *et al.* 1990; Bradshaw 1991; Larter *et al.* 2002; Eagles *et al.* 2004a; Wobbe *et al.* 2012).

From about 80 Ma, the Bellingshausen Plate started acting as an independently rotating plate, and continued to do so until about 61 Ma (e.g. Larter *et al.* 2002; Eagles *et al.* 2004a,b). Its incorporation into the Antarctic Plate occurred as part of a major plate reorganization in the South Pacific (Cande *et al.* 2000). Kipf *et al.* (2012) postulated that at around 65–56 Ma, the Marie Byrd Seamounts were formed from magmatic material that was transported from beneath the West Antarctic continental crust by a so-called continental insulation flow.

The eastern shelf, which contains Pine Island Bay, has been suggested by Dalziel & Elliot (1982), Storey (1991) and Grunow *et al.* (1991) as the site of a Palaeozoic–Mesozoic crustal boundary zone between the Marie Byrd Land block in the west and the Thurston Island crustal block in the east, whose apparent palaeomagnetic polar wander paths differ.

Recent analysis of magnetic and seismic data from the ASE shelf show that tectonic lineaments and sedimentary subbasins cross the shelf of which some may be related to a branch of the eastern West Antarctic Rift System (Gohl *et al.* 2013a,b). Apatite-He age trends, derived from rock samples of the eastern Pine Island Bay, infer rift-related block faulting indicating that the present glacially formed Pine Island Trough may have originated from tectonic activity as part of the West Antarctic Rift System (Lindow *et al.* 2011). Different thermal signatures of the Mt Murphy area and its neighbouring areas indicate a major fault system which was active during or after Oligocene (Lindow *et al.* 2011).

Latest geological studies in Marie Byrd Land show Cretaceous multistage rifting phases and strike slip faulting superimposed by transtension (Siddoway 2008). Gravity data, receiver-function analysis of teleseismic earthquakes and geological analysis suggest that the submarine plateaus of New Zealand and conjugate Marie Byrd

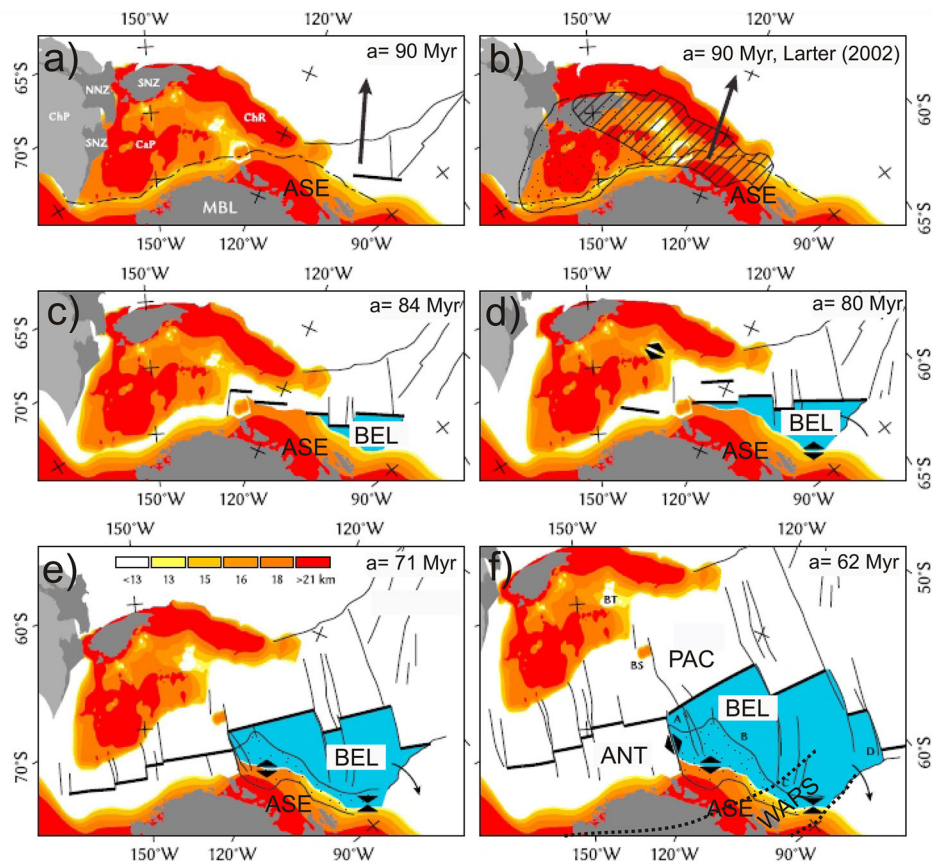


**Figure 2.** Pre-rift reconstruction model of distinct tectonic phases from the late Cretaceous to early Palaeocene of the Amundsen Sea Embayment including Chatham Rise (striated) and Campbell Plateau (stippled) modified after Wobbe *et al.* (2012) (Figs 2a, c–f) using the rotation parameters of Wobbe *et al.* (2012) and Grobys *et al.* (2008). Fig. 2(b) shows configuration using the rotation parameters from Larter *et al.* (2002). The black arrows in Figs 2(a) and (b) show the direction of movement of the Bellingshausen Plate. Thin black lines show fracture zones, thick black lines show mid ocean ridge segments. Thin black dashed line show suspected rift arm of the West Antarctic Rift System. Stippled area in Figs 2(e) and (f) shows oceanic crust which was formed along the Bellingshausen Plate margin. The colour scale in Fig. 2(e) shows the crustal thickness after modelling results of Wobbe *et al.* (2012). ANT, West Antarctic Plate; BEL, Bellingshausen Plate; BS, Bollons Seamount; BT, Bounty Trough; CaP, Campbell Plateau; ChP, Challenger Plateau; ChR, Chatham Rise; MBL, Marie Byrd Land; NNZ, North Island of New Zealand; PAC, Pacific Plate; SNZ, South Island; ASE, Amundsen Sea Embayment; WARS, West Antarctic Rift System.

Land consist both of thinned continental crust of only 25–28 km thickness (Lubes *et al.* 2003; Luyendyk *et al.* 2003; Winberry & Anandakrishnan 2004; Grobys *et al.* 2009). In the ASE, gravity modelling showed the crust of the inner to middle shelf to be of 24–28 km thickness. Moreover, it seems that the ASE was affected by magmatic intrusions interpreted from distinct zones of anomaly patterns and lineaments which can be associated with three major tectonic phases (Gohl *et al.* 2007, 2013a,b).

Jordan *et al.* (2010) calculated a Moho depth of about 19 km under the Byrd Subglacial Basin and the newly identified Pine Island Rift based on gravity inversion. Additionally, Bingham *et al.* (2012) also inferred crustal thinning leading to 25–21-km-thick crust beneath the Ferrigno rift and the adjacent Siple Trough region.

### 3 SEISMIC EXPERIMENT

The seismic data set presented in this study consist of two deep-crustal seismic refraction profiles and a suite of multichannel seismic reflection profiles (Fig. 1), that were acquired during RV Polarstern expeditions ANT-XXIII/4 in 2006 and ANTXXVI/3 in 2010. The seismic source used for both refraction and reflection recordings of the profiles AWI-20060100 and AWI-20060200 con-

sisted of 8 G-Guns (68.2 l in total) and a Bolt air gun (32 l). The shot interval of 60 s corresponded to an average shot spacing of 150 m. Additionally, seismic reflection profile AWI-20100119 was acquired with three GI-Guns, fired every 10 s (Gohl *et al.* 2013b). The multi-beam bathymetry was measured with the Hydrosweep DS-III system.

#### 3.1 Seismic reflection data

We mapped the top-of-basement along the refraction profiles AWI-20060100 and AWI-20060200, in coincident seismic reflection data (Fig. 1). These were acquired by using a 600-m-long analogue streamer with 96 channels. The data were recorded with a sampling interval of 4 ms. The data gap between the seismic reflection profiles AWI-20060100 and AWI-20060200 (Fig. 1) was bridged with the nearest seismic reflection profile

AWI-20100119 (Fig. 1) in order to generate an almost continuous transect. Data processing comprised CDP sorting with binning of 100 m, owing to the long shot interval for the profiles AWI-20060100 and AWI-20060200 and 25 m for the profile AWI-20100119, bandpass filtering of 10–200 Hz and a detailed velocity analysis followed by stacking and post-stack migration.

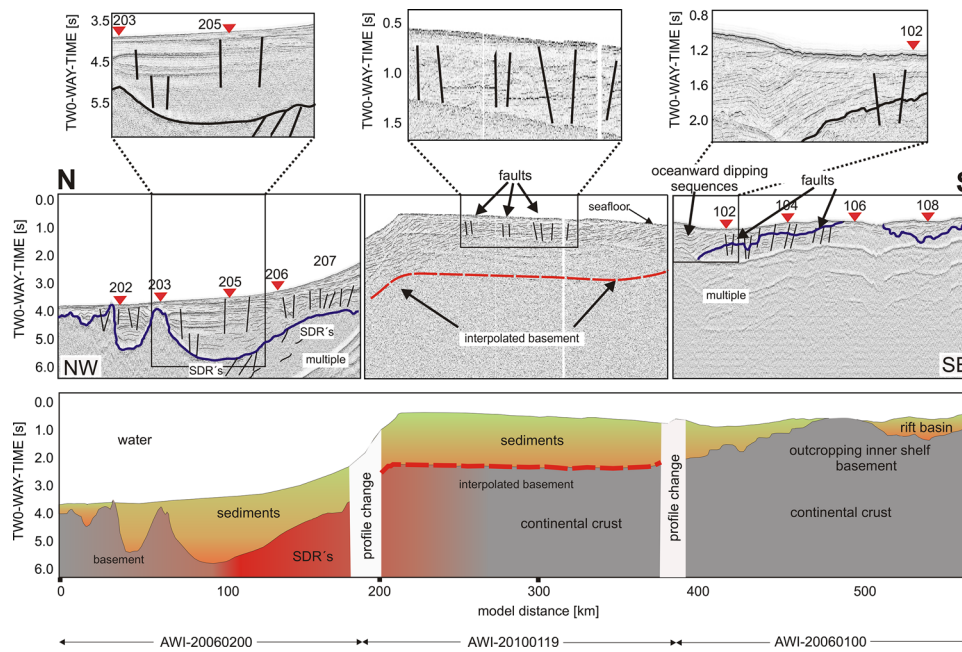


**Figure 3.** Compilation, line drawing and interpretation of seismic-reflection profiles AWI-20060100, AWI-20060200 and AWI-20100119 across the continental margin of the Amundsen Sea Embayment. The thick blue line indicates the interpreted top-of-basement. The dashed red line shows the interpolated top-of-basement based on a spectral analysis of free-air gravity data. The thin black lines within the sedimentary layer indicate unconformities, horst and graben and rift structures. Numbers including red triangles show the position of the OBH stations along the transect. The red lines indicate SDR, seaward dipping reflectors.

Attempts to suppress the shallow-water multiples on the shelf (Fig. 3) using techniques such as FK-filtering, Radon-transformation and predictive deconvolution produced minimal improvements due to the limited streamer length. Multiple suppression yielded, however, better results with the data of profile AWI-20100119 (Gohl *et al.* 2013b). We composed the three seismic reflection profiles into a single projected seismic transect (Fig. 3).

On the continental rise, the reflection data show stratified sediments to a two-way time of 2.5 s ( $\sim 3$  km depth) in the deepest basins. Below the sediments, the rise is dominated by seamounts of the Marie Byrd Seamount province. We observe indications of normal faults and horst and graben structures within the continental rise sediments. At the foot of the slope, some reflections beneath the top of the acoustic basement are reminiscent of the seaward-dipping reflectors (SDR) known for many passive continental margins of volcanic type. The top basement reflector disappears south of profile distance 160 km (AWI-20060200; Fig. 3) and beyond which strong seafloor multiples on the shelf and the slope mask deeper signals.

The seismic shelf records show that the basement is exposed on the inner shelf of the ASE (Fig. 3). Sediment sequences beneath the middle shelf dip seawards at  $0.5^\circ$ , and at  $1.5^\circ$  beneath the inner shelf. The outer shelf is dominated by large progradational sedimentary wedges (Gohl *et al.* 2013b).

### 3.2 Seismic refraction data and traveltimes modelling

Due to sea ice coverage, and in order to minimize the risk of instrument loss, only nine ocean bottom hydrophone (OBH) systems were deployed along the 165 km long profile AWI-20060100, with a regular interval of 18–19 km (Fig. 3). Four of the systems (OBH 102, 104, 106 and 108) recorded usable data. Along the 171-km-long profile AWI-20060200 (Fig. 1), seven OBH systems were deployed

with the same spacing between the Marie Byrd Seamount province and the foot of the continental slope (Fig. 3). Only five of these recorded usable data (OBH 202, 203, 205, 206 and 207). The raw OBH data were merged with the navigation data and then converted to SEG-Y format. The exact position of the OBH stations on the seafloor along the tracks were relocated by using direct  $P$ -wave arrivals. A bandpass filter of 4–20 Hz was applied to the seismic traces for reducing high and low frequent noise from the seismic signal.

We identify coherent  $P$ -wave phases of up to 120 km source-to-receiver offset at some stations (Fig. 4). All records show good-quality refracted  $P$ -wave phases from the crust (Pc1 and Pc2 phases; Fig. 5), some recordings contain high-amplitude wide-angle Moho reflections (PmP-phase) and intracrustal reflections (PcP-phase) as well as low-amplitude refracted phases from the upper mantle (Pn-phase). The Moho was identified as velocity contrast between the crustal layer and the upper mantle at velocities higher than  $8.0 \text{ km s}^{-1}$ .

We assigned a picking uncertainty of 150 ms to all  $P$ -wave arrivals. The traveltimes inversion software *RAYINV* (Zelt & Smith 1992) was then used for ray tracing to forward model the traveltimes branches, by applying a layer-stripping procedure from top to bottom. This was followed by a traveltimes inversion for fine-tuning the model parameters.

For the lower crust a resolution between 0.5 and 0.6 is reasonable at the shelf edge and continental rise, where 0 means no ray coverage and 1.0 represent maximum ray coverage (Fig. 7). Hence, the resolution of our  $P$ -wave models is the better in the upper and lower crust and the ray coverage is the densest at the middle section of both OBH profiles. Limited offsets lead to a lack of Pn- and PmP phases recordings at the ends of the profiles. The velocity distribution is laterally homogenous within the entire crust.

The velocity–depth model of profile AWI-20060200 (Fig. 6a) consists also of a sedimentary layer, upper and lower crustal

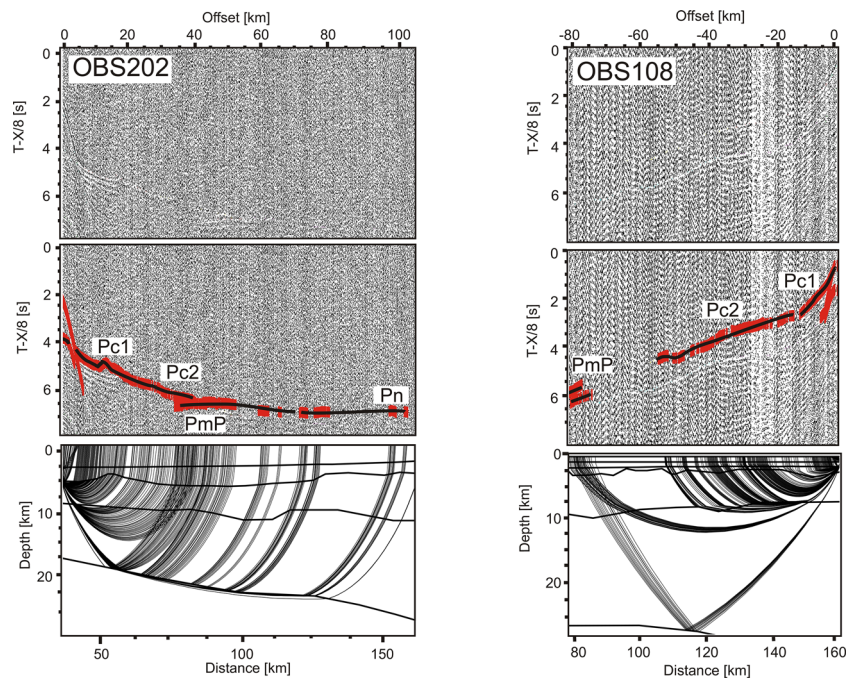


**Figure 4.** Top panel: part of seismic section from OBS 202 and 108, both plotted with a reduction velocity of  $8 \text{ km s}^{-1}$  and a bandpass filter of 4–20 Hz. Middle panel: Same section with modelled phases (black lines) and picked signals (red bars with bar length representing the pick uncertainty). Bottom panel: ray tracing results with ray coverage in the  $P$ -wave velocity model.

layers underlain by an upper mantle layer. Sediment velocities range from  $1.7$  to  $2.5 \text{ km s}^{-1}$  in the upper part to  $3.5 \text{ km s}^{-1}$  in the deepest basin. The depth to basement increases slightly towards the shelf. Two basement highs separate the area into three distinct areas (Figs 6a and b). In satellite-altimetry data (McAdoo & Laxon 1997), these highs correspond to circular features south of the Marie Byrd Seamount province. They probably therefore represent buried seamounts of the province. The northernmost area is around  $30 \text{ km}$  wide and  $1.0$ – $1.5 \text{ km}$  thick. A second area in the middle part of the profile is  $25 \text{ km}$  wide and filled with sedimentary rocks of around  $1.8 \text{ km}$  thickness. At the southern flank of the profile the largest basin is  $120 \text{ km}$  wide and the sediments are up to  $2.1 \text{ km}$  thick. The upper crust thickens slightly from  $3 \text{ km}$  in the north to  $6 \text{ km}$  at the southern profile end.  $P$ -wave velocities in the upper crust range from  $5$  to  $6 \text{ km s}^{-1}$ . The lower crust also thickens slightly southward, from  $7 \text{ km}$  in the northern ASE to around  $13 \text{ km}$  towards the shelf. The crust-mantle boundary (seismic Moho) can be identified at a depth of  $14 \text{ km}$  in the north, which increases to  $23 \text{ km}$  near the foot of the continental slope.

Lower crustal velocities range from  $6 \text{ km s}^{-1}$  at the top of the layer to  $7 \text{ km s}^{-1}$  at its base in the north and  $7.7 \text{ km s}^{-1}$  in the south. The seismic Moho can be recognized at the base of the lower crustal high velocity layer by upper mantle velocities larger than  $8 \text{ km s}^{-1}$ .

The data of OBH profile AWI-20060100 (Fig. 6b) were inverted to yield a 2-D velocity–depth model that comprises a sedimentary layer, and upper and lower crustal layers underlain by the uppermost mantle. We identify five distinct sedimentary basins with variable ( $0.7$ – $1.5 \text{ km}$ ) fill thickness and velocities ranging between  $1.7$  and  $3 \text{ km s}^{-1}$ . The upper crust is between  $4.1$  and  $6.3 \text{ km}$  thick with  $P$ -wave velocities ranging from  $5$  to  $6.2 \text{ km s}^{-1}$ . The lower crustal thickness increases southward from  $14 \text{ km}$  in the north to  $24 \text{ km}$  beneath the inner shelf. Velocities in this layer range between  $6.2$  and  $7.1 \text{ km s}^{-1}$  in northern part and between  $7$  and  $7.6 \text{ km s}^{-1}$  in the southern part. The seismic Moho was identified at depths between

$25$  and  $30 \text{ km}$ . Similar ss on profile AWI-20060200, the seismic Moho is identified at the base of the lower crustal high velocity layer.

#### 4 GRAVITY ANOMALIES AND MODELLING

The interpretation and modelling of potential field data is carried out to investigate regional geological issues and to highlight deep and shallow crustal anomalies as well as basin structures. A joint interpretation of profile-based seismic data with free-air gravity anomaly (FAA; Fig. 8a) and Bouguer anomaly (BA; Fig. 8b) grids sets the seismic data into a regional geological context.

We calculated the BA of the area between  $75^\circ\text{S}$ – $71^\circ\text{S}$  and  $100^\circ\text{E}$ – $120^\circ\text{E}$  by using the satellite derived FAA of McAdoo & Laxon (1997), the latest bathymetry grid of Nitsche *et al.* (2007) (Fig. 1) and a Bouguer reduction density of  $2.67 \text{ g cm}^{-3}$ .

Additionally, we used the spectrum of the gravity data to fill the data gap between the seismic refraction profiles AWI-20060100 and AWI-20060200, which exhibits a prominent gravity anomaly high. This high is similar to those observed close to various shelf breaks worldwide, which can be related to various density contrasts including those resulting from crustal thinning, thick accumulations of sediments, and magmatic underplating (Watts & Fairhead 1999).

However, in order to calculate the depths of significant density interfaces in our data gap, we applied the power spectral analysis based on the method of Spector & Grant (1970) to the FAA of McAdoo & Laxon (1997). The method was developed for magnetic data and adapted for gravity data by Karner & Watts (1983). The method is based on the assumption of geological interfaces that are essentially horizontal with some small relief. With this assumption, the power spectrum of a group of prismatic sources distributed over the subsurface topography reveals a quasi-linear relationship between the power spectral density (PSD) and the wavenumber  $k_r$ . In

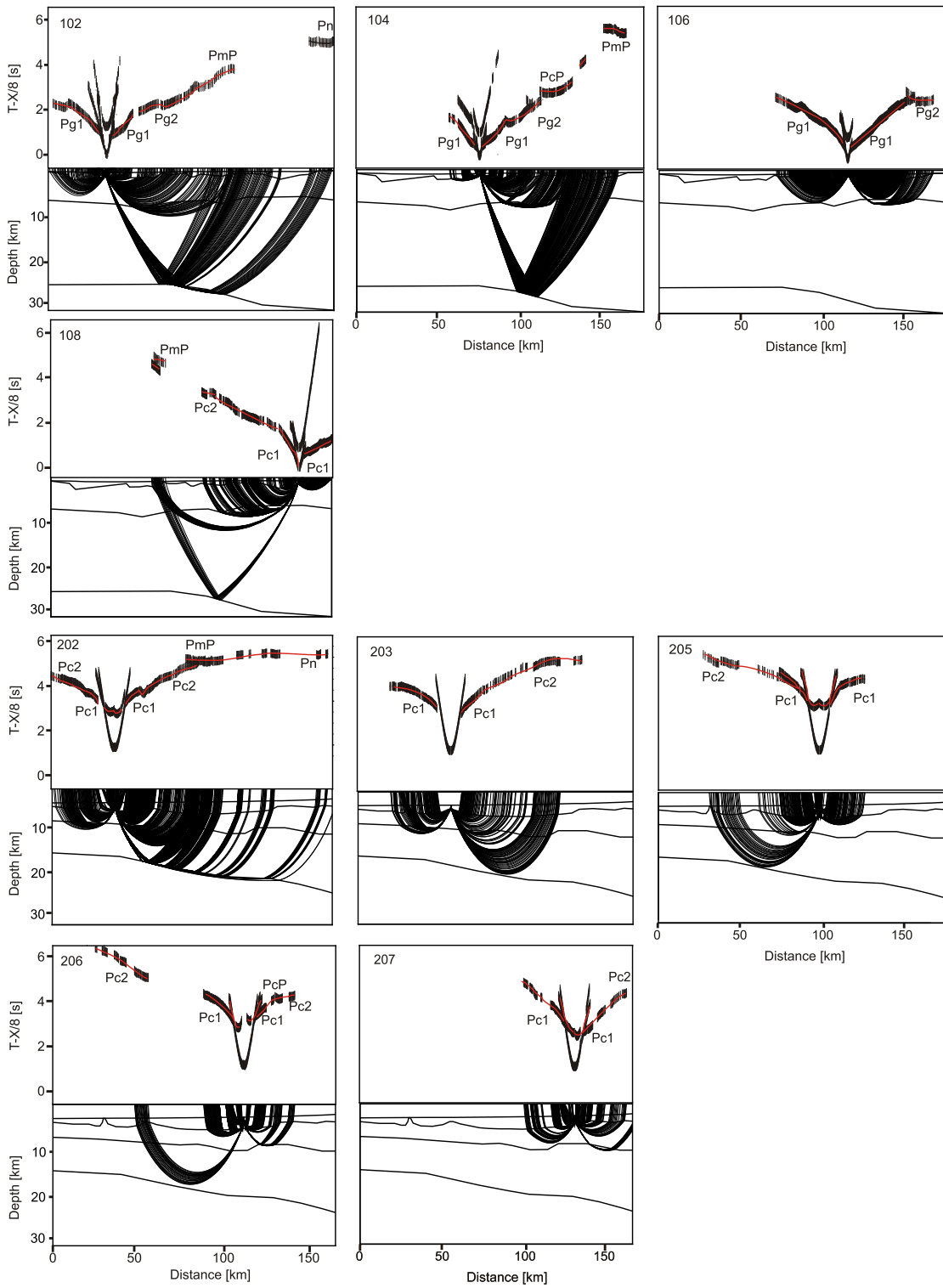


**Figure 5.** Comparison of picked and computed traveltimes branches from the  $P$ -wave velocity models for each OBH station combined with the corresponding ray path. Depth is annotated in kilometres, the sections are plotted with a reduction-velocity  $T-X/8$  in (s). The error bars indicate observed picking times and the size of the bars corresponds to the picking uncertainty. Solid red lines show the calculated traveltimes. Near-offset phases ( $P_{sed}$ , direct waves) are not annotated. Position of each OBH along the profiles is shown in Fig. 3.

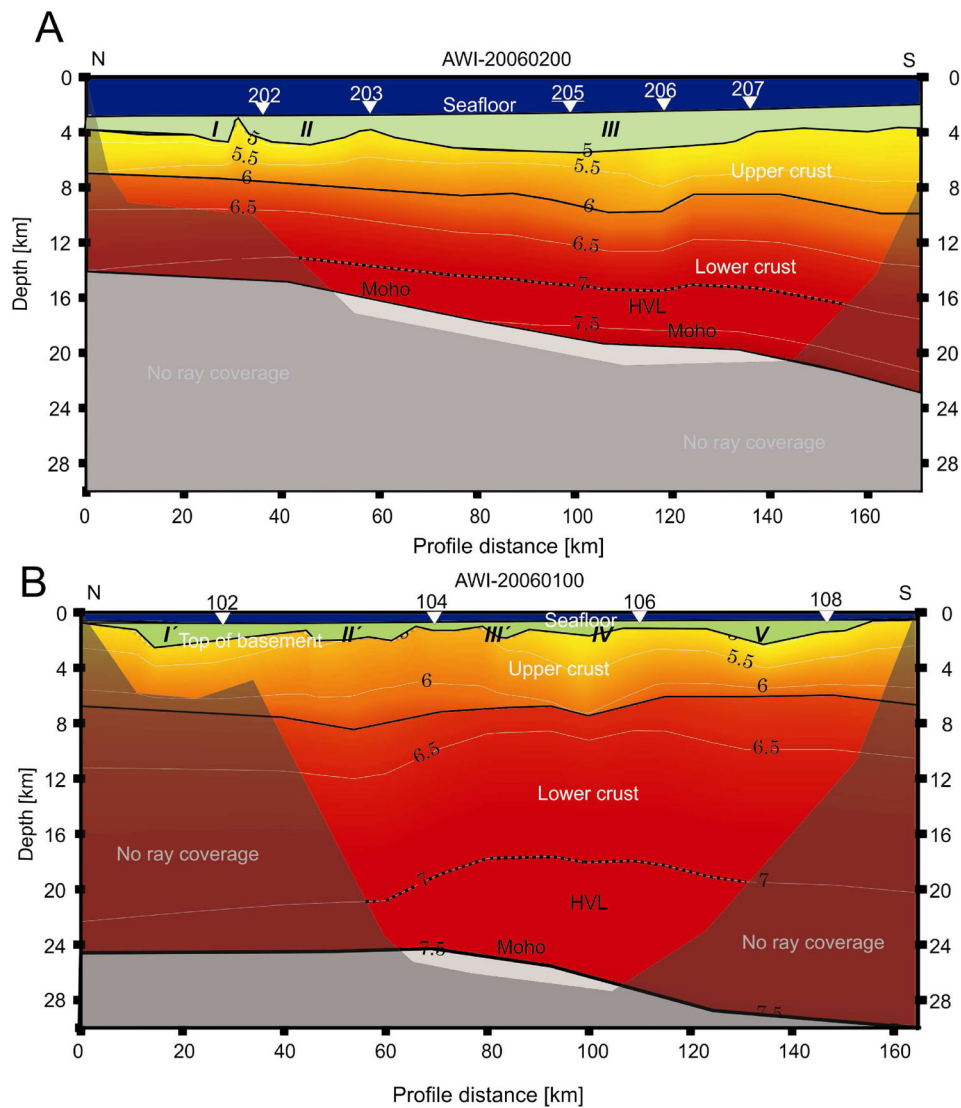


**Figure 6.** Final  $P$ -wave velocity models of the seismic refraction profiles. (b) AWI-20060100 (bottom) and (a) AWI-20060200 (top). The models are overlain by a semitransparent mask showing areas without ray coverage. Numbers and triangles show the OBH stations along the profiles. I, II, III and I', II', III', IV and V label sedimentary basins along the profiles.

a plot of the natural logarithm of the FAA's power spectrum against  $k_r$ , a set of distinct linear segments is related to the mean anomalies of the mass anomaly. The slope of a linear segment multiplied by  $-0.5$  yields the mean depth to its source. The window used for the spectral analysis covers an area of  $200 \text{ km}^2$  and is a compromise between uniform size and area (Fig. 1). The chosen area should contain provinces of uniform geology, but on the other hand should be large enough to resolve longer wavelengths and therefore greater depths.

#### 4.1 Satellite-derived free-air gravity anomalies

The FAA of the outer shelf is dominated by two highs of up to  $80 \text{ mGal}$  which correspond to the bathymetrically elevated Western and Eastern Outer Banks (Gohl *et al.* 2013b). Over the middle shelf area, we identify a major WSW–ENE trending negative anomaly with a minimum of  $-70 \text{ mGal}$  and name it the Amundsen Sea Embayment Low (ASEL). This anomaly is interrupted by the so-called Peacock Gravity Anomaly (PGA) that is northwest–southeast orientated (Eagles *et al.* 2004a) and which continues to Thurston Island

(TI) as the Thurston Island Low (TIL). Pine Island Bay (PIB) is divided by the north-striking glacial Pine Island Trough (PIT) with a gravity low of  $-50 \text{ mGal}$  (Fig. 8).

#### 4.2 Satellite derived BAs

The gravity effect of topography and bathymetry is removed from the FAA to generate the BA such that only information on rock density variations is retained. At long wavelengths, the transition from oceanic to continental crust can be clearly identified from a pronounced southward decrease of the BA from  $140$  to  $40 \text{ mGal}$  (Fig. 8b). The inner shelf is characterized by shorter wavelength anomalies of between  $0$  and  $70 \text{ mGal}$  whereas the outer shelf shows predominantly long wavelength anomalies of between  $-20$  and  $70 \text{ mGal}$ , that correlate with bodies identified in a recent magnetic analysis of the ASE (Gohl *et al.* 2013a). We also identify a significant BA high larger as  $60 \text{ mGal}$  in the PIB region. As in the FAA, the ASEL and TIL appear as a WSW–ENE trending low dominating the middle shelf (Fig. 8b) which is interrupted by a positive WNW trending anomaly of up to  $70 \text{ mGal}$  corresponding to the PGA.

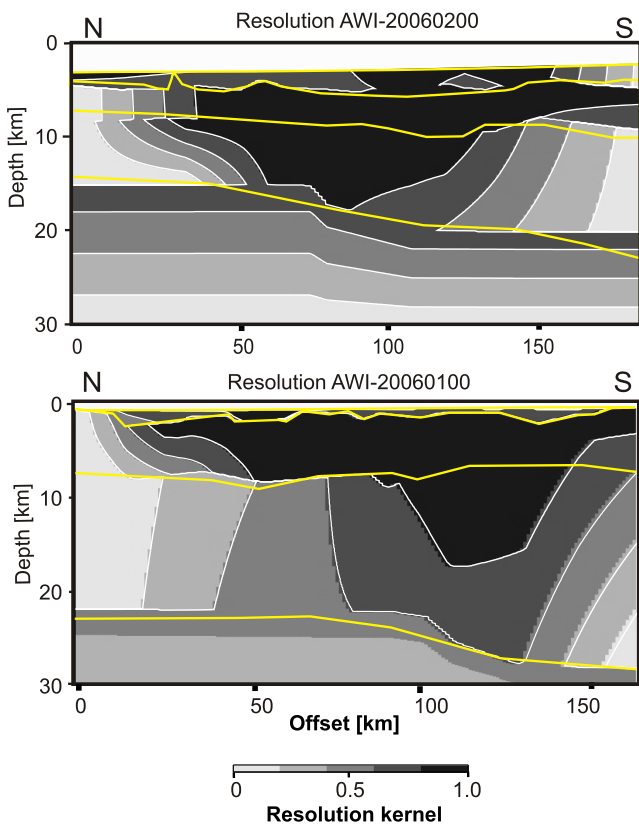


**Figure 7.** Resolution values of the two seismic traveltime inversion models for the  $P$ -wave velocity–depth models (B) AWI-20060100 (bottom) and (A) AWI-20060200 (top). The grey shading corresponds to the resolution value. Resolution values of greater than 0.5 indicate a moderate to good resolution. The yellow lines show the layer boundaries from the corresponding velocity–depth model. Contour lines are plotted at an interval of 0.2.

The outer shelf area is dominated by a major gravity low which we name the Outer Low. The boundary between the outcropping basement in the south and the sedimentary basin on the shelf corresponds to a change in the BA from 0 to 50 mGal. At least a prominent BA high up to 60 mGal over the PIB can be identified.

### 4.3 Spectral analysis results

Spectral analysis for the gap between the two seismic refraction profiles (Fig. 1) reveals two distinct linear segments for which linear regressions suggest a deeper and a shallower interface (Fig. 9). The choices of endpoints for the linear regression were made by visual inspection. The slope of the low-frequency (deeper) segment **A** corresponds to a mass anomaly depth of  $22 \pm 2$  km whereas the slope of high-frequency (lower) segment **B** corresponds to an anomaly depth of about  $4 \pm 2$  km. The uncertainty of the depths of the interfaces is controlled by the sampling interval of the spectral analysis and can be estimated to be around 2 km for crustal depths (Ciancara & Marcak 1976).

## 5 SHIP-BORNE GRAVITY DATA AND 2-D MODELLING

### 5.1 Data processing and description

Shipborne gravity data were collected continuously along all profiles with a KSS-31 sea gravimeter at a sampling interval of 1 s. The

raw data were corrected for instrument drift during the cruise by using reference measurements in Punta Arenas, Chile. We reduced the data to FAA with respect to the GRS80 gravity model using a standard processing procedure (Torge 1989), including an Eötvös correction calculated with the ships navigation. The  $\sim 200$ -km-wide data gap between profiles AWI-20060100 and AWI-20060200 was filled using the free air gravity data of McAdoo & Laxon (1997).

The gravity anomaly decreases linearly from model distance 0–150 km from  $-10$  to  $-70$  mGal (Fig. 10). Two short wavelength undulations of a few mGal in the north correlate with the buried seamounts in the seismic data (Fig. 3). Across the shelf edge, the FAA increases up to 50 mGal at profile distance 250 km. This gravity high is similar to other observations at various shelf breaks, named the ‘sedimentation anomaly’ according to Watts & Fairhead (1999). If a 2-D model profile is oriented perpendicular to the shelf break the density contrast between the sediments and the water is sufficient to model the anomaly. As our profile runs more or less perpendicular to the shelf edge (Fig. 1), it is likely that a 3-D effect of the shelf break contributes to the upward anomaly. Over the middle shelf, the FAA reaches a local minimum of  $-50$  mGal at 400 km profile distance and increases up to 20 mGal towards the inner shelf.

### 5.2 2-D Density–depth modelling

We used the software *IGMAS* (Götze & Lahmeyer 1988) to model a composite FAA transect. To calculate the 2-D gravity effect of a mass anomaly, the *IGMAS* algorithm uses triangulated polyhedra built from a set of polygons defined in parallel vertical cross sections. The triangulation between these vertical planes is done automatically during the modelling procedure. We defined polygons using ship-borne bathymetry data, seismic refraction and seismic-reflection data along profiles AWI-20060100, AWI-20060200 and AWI-20100119, and the results of the spectral analysis in order to setup a starting model. The model geometries at the ends of the profiles were edited to account for the regional gravity field. To simplify the model, we combined all observed sedimentary units into one layer and calculated an average density of  $2050 \text{ kg m}^{-3}$  using the velocity–density relationship of Nafe & Drake (1963). As the observed  $P$ -wave velocities of the crust indicate continental affinity along the modelled profile (Christensen & Mooney 1995) we used the velocity–density relationship of Barton (1986) to define upper-crust density of  $2650 \text{ kg m}^{-3}$  and a lower-crust density of  $2800 \text{ kg m}^{-3}$ . Finally, we modelled the observed high-velocity layer with a density of  $3150 \text{ kg m}^{-3}$ , also after Barton (1986). The upper-most mantle was modelled with a density  $3300 \text{ kg m}^{-3}$ . During the modelling procedure, we compared the density with results of the  $P$ -wave velocity–depth models and adjusted every layer boundary to obtain a best fit between the measured and modelled anomaly by varying the crustal geometry as little as possible.

Owing to the inherently non-unique testimony of gravity signals, we present two models that each explain the observed anomaly (Fig. 10). The standard deviation between the measured and modelled FAA in model A is 1.53 mGal along profile AWI-20060100 and 1.32 mGal along profile AWI-20060200 including the interpolated part. With model B, these values are 1.53 and 2.01 mGal. In general, the correspondence between the velocity–depth and density–depth models is acceptable.

In its central part (Fig. 10) the model suffers from the absence of seismic-reflection data and a velocity–depth model. We constrained the range of models applicable to this part using the results of the power-spectral analysis of its FAA field. As noted above, this part of

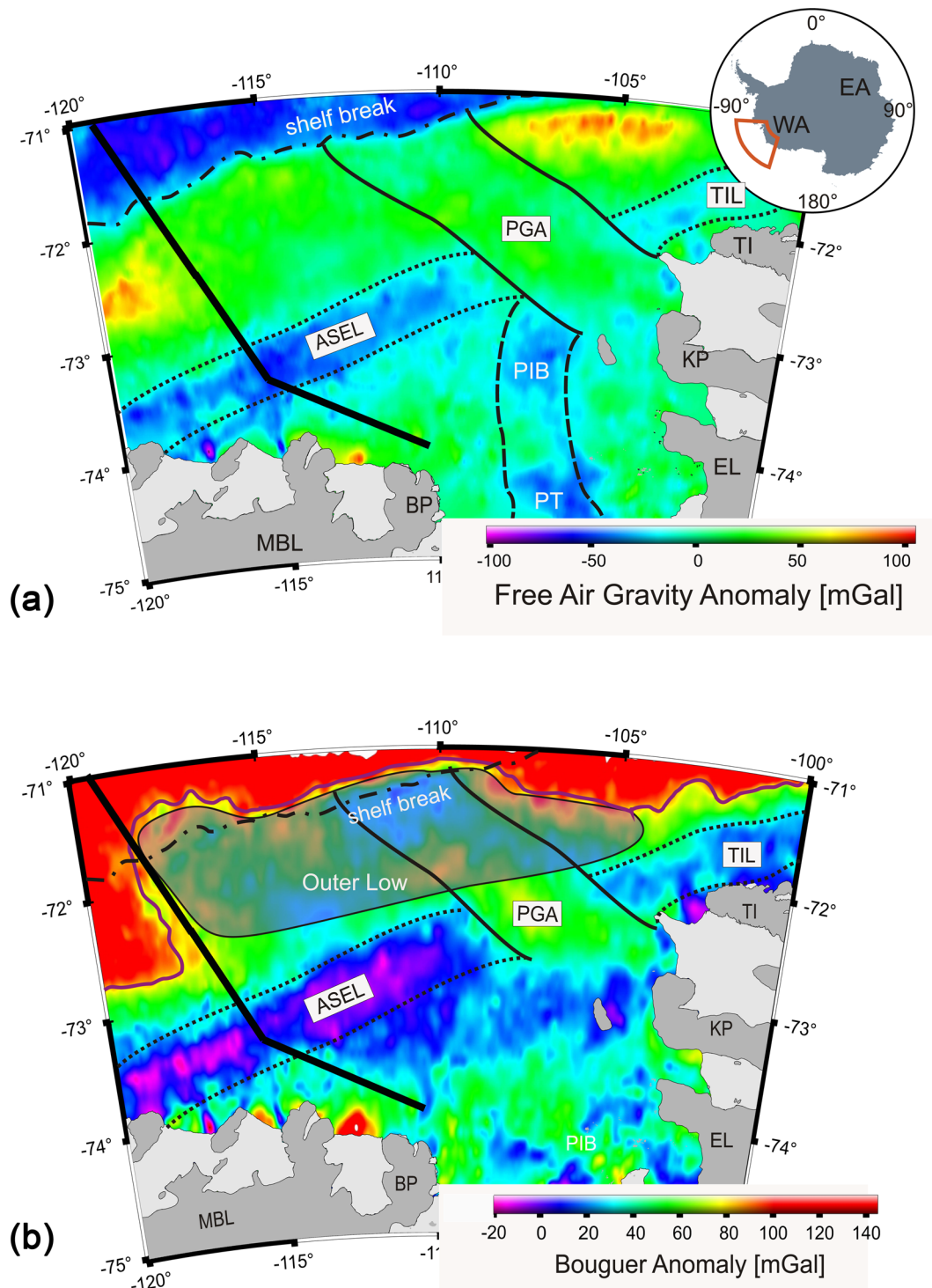


**Figure 8.** Compilation of gravity data. (a) Maps the satellite-derived free-air gravity anomaly of the Amundsen Sea Embayment (McAdoo & Laxon 1997). The thin black dotted and continues lines mark prominent gravity anomalies along the middle and outer shelf of the Amundsen Sea Embayment. (b) Images the calculated Bouguer Anomaly. The framed semi-transparent area beneath shelf break shows a prominent low (Outer Low). The thick black dotted line marks the 2-D gravity rise-to-shelf model transect (Fig. 10). ASEL, Amundsen Sea Embayment Low; TIL, Thurston Island Low; PGA, Peacock Gravity Anomaly; PT, Pine Island Trough; BP, Bear Peninsula; MBL, Marie Byrd Land; EL, Ellsworth Land; TI, Thurston Island; KP, King Peninsula.

the profile crosses the gravity high of the Western Outer Bank (Gohl *et al.* 2013a). In model A, the sedimentary layer is up to 3 km thick, consistent with the power spectral analysis. The top-of-basement interface is rough south of the gravity high at profile distance of 300–370 km. The Moho steps down from a depth of about 22–27 km

between profile distance 170–200 km, again consistent with the power spectral analysis, and remains at this depth until after profile distance 400 km, where it is constrained once again by refraction results on profile AWI-20060100. With these layers, it becomes necessary to model the gravity high as the signal from a 10 km high

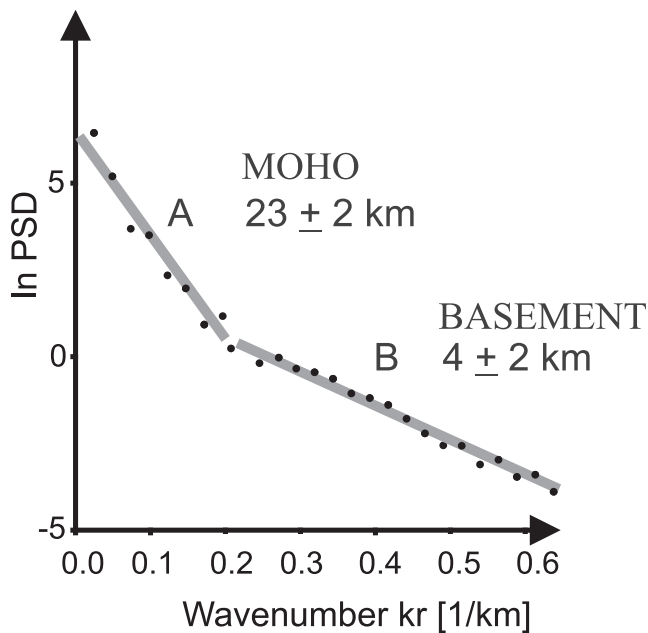


**Figure 9.** Spectral analysis of the satellite-derived free air gravity anomaly of McAdoo & Laxon (1997). The natural logarithm of the energy spectra (PSD) in  $\text{mGal}^2\text{km}$  is plotted against the wavenumber in  $\text{km}^{-1}$ . The black dots show the values of the energy spectra and the grey line is the result of a linear regression for the depth estimation. The slope of the regression line corresponds to the anomaly mass depth. Anomaly mass depth is presented in km. Line A show the low frequency area (wavenumber lower than  $0.1 \text{ km}^{-1}$ ) and line B the high frequency area.

bulge in the high-density/high-velocity layer of the lowermost crust between profile distance 210–370 km. In model B, the high can be explained by thinning of the sedimentary layer between profile distance 170–250 km, and its absence between profile distance 250–370 km, although this latter depiction is not consistent with the power spectral analysis. The high-density layer is 4–7 km thick with no significant bulge.

## 6 DISCUSSION

### 6.1 Crustal structure

The FAA predominantly reflects the seafloor topography (Fig. 8a), whereas the BA portrays density and thickness variations of the lithosphere, including the gradual negative gradient that indicates the transition from continental to oceanic crust (Fig. 8b). However, our transect lies mostly within the interpreted continental crust. The Outer Low of the ASE shelf correlates with an elevated basement identified in seismic-reflection data from the ASE, named the Western Outer Bank (Gohl *et al.* 2013b). Contrary to the FAA, the corresponding BA signal reaches into the continental rise indicating that its source is not topographic (Fig. 8). The corresponding BA signal is probably the gravimetric signal of a thicker continental sliver generated during the Cretaceous extension that led to the separation of West Antarctica and Zealandia.

We subdivide the crust of the ASE into an upper crust, a lower crust and a high velocity lowermost crustal layer. The average upper crustal  $P$ -wave velocity of around 5.5 km/s along the entire transect is typical of uppermost continental crust (Christensen & Mooney 1995; Fig. 10). The absence of any  $P$ -wave velocity or density

variations below the two Marie Byrd seamounts indicates that these basement highs consist of similar material as the surrounding crust. The northern end of profile AWI-20060200 is less certain due to the lack of ray coverage and reversed records.

In general, the lower crustal  $P$ -wave velocities and densities are greater than expected for normal continental crust indicating a more mafic crustal composition (Christensen & Mooney 1995). Between model distances 180–380 km, our models are not constrained by deep seismic data. However, based on the gravity spectral analysis and an adjacent seismic-reflection profile, we argue that the sedimentary layer and the upper and lower crust have architectures similar to those beneath the continental slope and the inner shelf. The modelled rougher basement explains the high-frequency variations of the FAA. In Model A the estimated depth to top basement fits better to the flanking seismically constrained profiles than Model B, suggesting that its geometry is more appropriate to describe the ASE.

### 6.2 High-velocity layer

Traveltime modelling reveals  $P$ -wave velocities of 7.0–7.6  $\text{km s}^{-1}$  in the lower crust along both seismic refraction profiles corresponding to densities between 3140 and 3160  $\text{kg m}^{-3}$  in the gravity models (Barton 1986). These densities differ significantly from those expected for normal upper mantle density (3300  $\text{kg m}^{-3}$ ) or for normal lower continental crust (Anderson 1989). The maximum 10 km thickness of this layer is comparable to the thickness of high-velocity bodies known from other extended and volcanic type continental margins like the East Greenland continental margin (Voss & Jokat 2007) or its conjugate Vøring margin offshore mid-Norway (Mjelde *et al.* 2002). In these settings, the high-velocity bodies are interpreted as underplating of gabbro by accumulation of magma at the Moho during extension. By analogy, therefore we propose that the high-velocity layer beneath the ASE may represent widespread magmatic underplating (Fig. 10) indicating that the margin is of volcanic-type rather than of magma-poor type (Mutter *et al.* 1984). Hints of SDRs farther north reinforce the notion that the breakup process between greater New Zealand and West Antarctica was accompanied by magmatism. Grobys *et al.* (2009) interpret the observed high-velocity body of the conjugate southern Bounty Trough off eastern New Zealand as a mafic body intruded into the lower and upper crust and its high-velocity zone, as possible underplating at the base of the crust. However, the continental margins of eastern Zealandia, the Chatham Rise and the Campbell Plateau are not characterized well enough to match the categories of volcanic or non-volcanic type margins due to the lack of deep crustal data.

If the SDRs found along line AWI-20060200 (Fig. 3) of the Amundsen Sea do not find a counterpart on the New Zealand margin, the Amundsen Sea SDRs may be sequences of post-breakup volcanic phases. A study of the Southeast Greenland margin of Hopper *et al.* (2003) reports volcanic seaward dipping reflectors on oceanic crust, 180 km seaward of the continent-ocean-boundary which suggests that SDRs are not necessarily related to initial break-up.

Kipf *et al.* (2012) propose the generation of magma from partial melting of upper mantle rocks convecting as part of a so-called continental insulation flow on the basis of HIMU-type magmatic rocks (high time-integrated  $^{238}\text{U}/^{204}\text{Pb}$ ) from beneath the Marie Byrd Land to the present-day Marie Byrd Seamount province between Late Cretaceous and Palaeocene. They suggested the upwelling arm of the convection cell exists beneath Marie Byrd Land at the present-day. This hypothesis suggests an alternative source

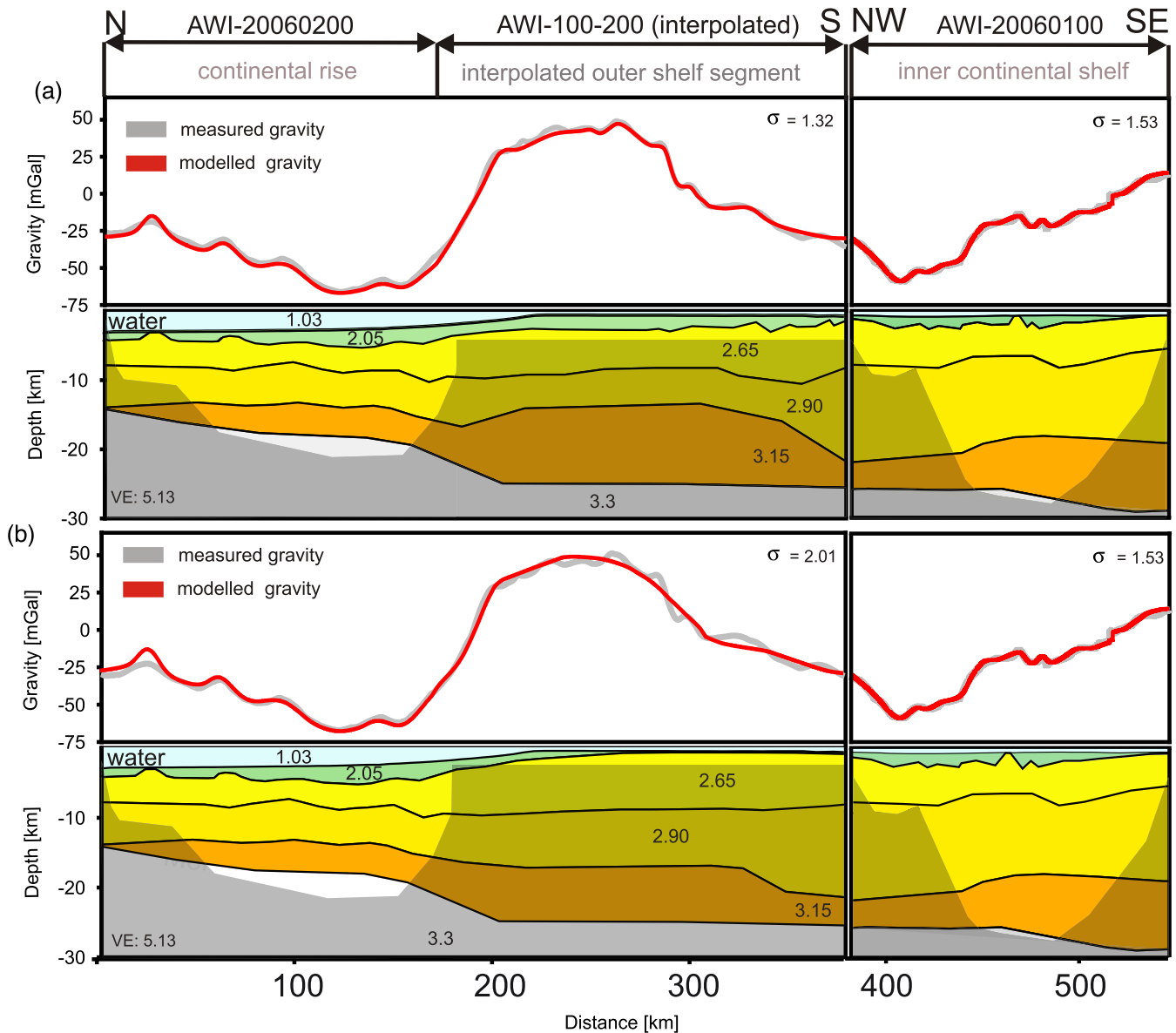


**Figure 10.** Two different 2-D forward gravity models of the seismic refraction profiles AWI-20060100 and AWI-20060200. The data gap between the two seismic refraction profiles was bridged with satellite-derived gravity data from McAdoo & Laxon (1997) and modelled using constraints from spectral analysis of the satellite-derived gravity data of McAdoo & Laxon (1997) and the adjacent seismic reflection profile AWI-20100119 (Fig. 2). Bathymetric surface is after Nitsche *et al.* (2007). Density values are given in  $10^3 \text{ kg m}^{-3}$ .

of gabbroic lower crust on the ASE shelf, in direct proximity to the Marie Byrd Land Seamount province.

However, if the bulge would be constituted by gabbroic melt, the expected density would be around  $2800 \text{ kg m}^{-3}$ , which is significant lower than the observed  $3150 \text{ kg m}^{-3}$ .

In the end the density of the HVL is too high for magma of Phanerozoic origin. On the other hand, the occurrence of cumulated layers could significantly rise the density of the material.

### 6.3 Serpentinization

An alternative explanation for the HVL is serpentinization of mantle material (e.g. Carlson & Miller 2003). Serpentinized peridotite can have velocities and densities similar to those of lower continental crust (Boillot *et al.* 1992). Serpentinite was observed along many non-volcanic passive margins such as the West Iberian margin

(Boillot & Winterer 1988; Whitmarsh *et al.* 1996) or the Newfoundland margin (Reid 1994). Boillot *et al.* (1992) suggested that the formation and accretion of serpentinite beneath the crust may play a role in areas of rifted continental margins.

However, in these settings serpentinization requires the penetration of seawater downward via faults, and low-angle detachment surfaces. Another possibility is via deep hydrothermal circulation. Hydrothermal activity was observed at intraplate volcanoes such as the Lo'ihi volcano (Malahoff *et al.* 2006). The Marie Byrd Seamount province is identified as a system of intraplate volcanoes (Kipf *et al.* 2012). Hence, the crust of this area has a potential for seawater penetration.

Serpentinization is a gradual process creating no clear boundary between unaltered peridotite and serpentinized mantle material. Magma-poor margins are often characterized by an increasing  $P$ -wave velocity from the crystalline basement to the mantle without

a clear Moho response due to serpentinized mantle material (Minshull 2009). At the West Iberian margin, the absence of clear Moho reflections were interpreted as the result of partial serpentinized mantle peridotite (Chian *et al.* 1999).

Mjelde *et al.* (2002) discussed the possible occurrence of serpentinized mantle in combination with magmatic underplating along the Vøring volcanic passive margin offshore mid-Norway. The observation of clear Moho reflections was the key argument for favouring the underplating hypothesis (Mjelde *et al.* 2002). We modelled the observed HVL with a density of  $3300 \text{ kg m}^{-3}$  and hence, of significant higher density than the average density of serpentinite at this depth (Christensen 1996). We therefore imply a continental margin that is likely more influenced by magmatism than undercrusted by serpentinite.

#### 6.4 Tectono-magmatic evolution

The seismic reflection data of the ASE reveal dipping lowermost strata on the inner ASE shelf, which may represent the earliest sedimentary rocks in the Amundsen Sea (see also Gohl *et al.* 2013b). We interpret the different northward dipping sedimentary reflectors as probable results of different extensional phases during the formation of the area. Normal faults indicate crustal extension affected the area. The present-day crustal architecture beneath the shelf infers wide-mode rifting such as observed in the Basin and Range Province of western North America (Hamilton 1987) rather than narrow-mode rifting such as the east African Rift System (e.g. Ebinger *et al.* 1989; Buck 1991; Rosenbaum *et al.* 2002) but the existence cannot be excluded from our data. Horst and graben structures are a further indication that the region evolved by wide-mode rifting (Buck 1991). Fault-like structures on the shelf may represent block-faulting during early stage and aborted rifting. The BA of the ASE shelf (Fig. 8b) shows several pronounced local highs and lows suggesting a pattern of rift basins and intervening highs. It is possible to speculate that the basins in the ASE (Fig. 3) are related to the pre-breakup dextral transtensional strain known from western MBL (Siddoway 2008) which is a hint for activity of the WARS affecting the entire ASE. A southward decrease of the BA with a gradient of about  $1.5 \text{ mGal km}^{-1}$  may also indicate that the crust was affected by rifting. The WSW-ENE trending ASEL and TIL strike parallel to the Pacific Antarctic Ridge in the north and the Bentley Subglacial Trough in the south and where our model crosses the ASEL it shows a thinned, 20-km-thick continental crust.

We interpret these observations as a record of a multistage initial Cretaceous wide-mode rifting event and thermal subsidence that followed the eventual successful breakup Zealandia from Antarctica. Our data show evidence for crustal extension connected to activities of the WARS since Cretaceous that resulted in the abandonment or evolution of a young-stage wide rift zone in favour of a fully developed extended continental margin and mature oceanic crust. It is possible that this rifting is connected to the well documented distributed Cenozoic extension superposed by narrow mode extensional events within the eastern Ross Sea sector of the WARS and the onshore parts of the ASE (Luyendyk *et al.* 2003; Davey & De Santis 2006; Jordan *et al.* 2010). However, the absence of implications for narrow-mode rifting in the offshore part of the ASE is not in conflict with this interpretation.

The orientation of lineaments in potential field data infer that these rifting events continued to affect the ASE after breakup from Zealandia, becoming a site for Bellingshausen-West Antarctic and East Antarctic–West Antarctic Plate divergence in Palaeocene and Oligocene times (Eagles *et al.* 2004a; Gohl *et al.* 2013a).

Fig. 11 presents a schematic tectono-magmatic reconstruction of the continental margin segment sampled by our model from late Cretaceous breakup of New Zealand and West Antarctica until Oligocene times (Figs 11e to b) and the present-day configuration (Fig. 11a). Fig. 11(e) shows the possible lithospheric configuration during or short before breakup between New Zealand and West Antarctica at around 100 Ma.

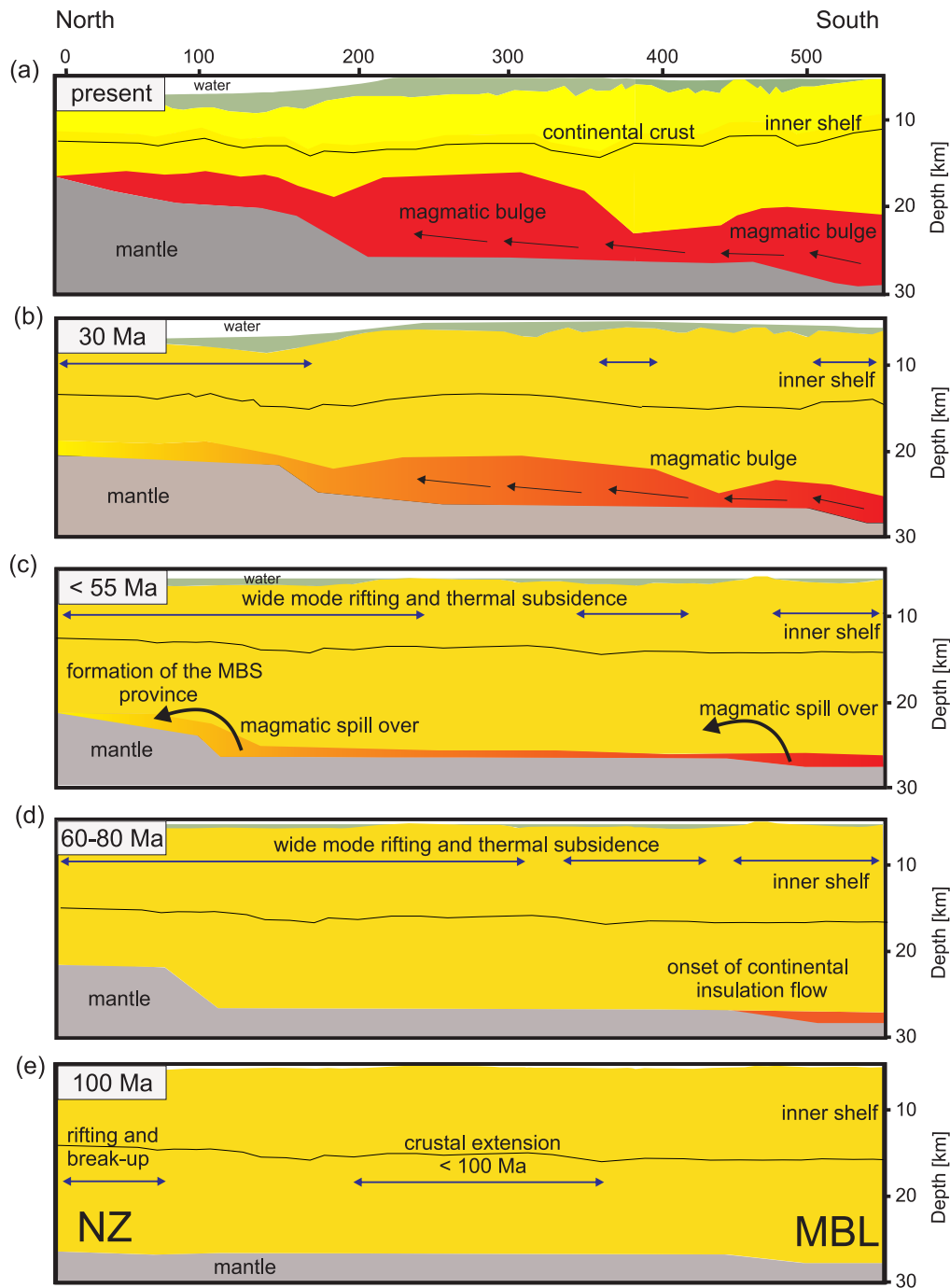
The crustal architecture was homogenous along the entire profile. At this time, extension may start between Zealandia and West Antarctica. Mukasa & Dalziel (2000) inferred subduction-related I-type magmatism occurred at least until  $94 \pm 3 \text{ Ma}$  (U-Pb zircon date) from the Walgreen Coast–eastern MBL (Fig. 1) to western Pine Island.

Fig. 11(d) shows the possible configuration during onset of wide-mode rifting between 60 and 80 Ma. We infer the onset of magmatism at this time based on magmatic flow estimations as discussed above. Fig. 11(c) images ongoing magma flow, the occurrence of the Marie Byrd Seamount province which was accompanied by thermal subsidence of the palaeo shelf of the ASE. The time slice shown in Fig. 11(b) illustrates the lithospheric configuration during 30 Ma. Ongoing magma accumulation was accompanied by tectonic rifting. At least Fig. 11(a) illustrates the present-day configuration. The reconstruction is based on the crustal architecture of our gravity and seismic model (Fig. 10b). The basin development we illustrate at the top surface of our transect is based on a schematic back-stripped reconstruction applied for the ASE shelf by Gohl *et al.* (2013b).

Due to the absence of evidence for a volcanic extended margin south of Zealandia, we prefer to explain the magmatic underplating as a product of partial melting during convective mantle flow set up by long-lived continental insulation. There are no robust constraints about the timing of this flow but Kipf *et al.* (2013) propose the formation of the Marie Byrd Seamounts to be in Early Cenozoic ( $\sim 56 \text{ Ma}$ ). With respect to the present-day distance of around 800–1000 km between the central Marie Byrd Seamount province and coast of eastern Marie Byrd Land (Fig. 1) and an average convective velocity of around  $1\text{--}5 \text{ cm a}^{-1}$  (Schubert *et al.* 2001), the onset of magma flow may have occurred around 10 Myr earlier at about 65 Ma. This is consistent with a suspected major plate reorganization in the South Pacific in Palaeocene (Cande *et al.* 2000).

Further, the assumed increasing magmatic activity beneath the ASE shelf shown in Fig. 11(b) at about 30 Ma correlates with the emplacement age of the Dorrel Rock intrusive complex in Marie Byrd Land (Rocchi *et al.* 2006) implying that a major or several single magmatic events related to multistage tectonic activity affected the Amundsen Sea margin. Additionally, the observation of different thermal signatures in the Mt Murphy area of western Marie Byrd Land, which indicate a major fault system and which was active during or after the Oligocene (Lindow *et al.* 2011) is an implication for tectonic activity in this region. We interpret this as a further indication that tectonic and magmatism were coupled processes during the Oligocene and are related to the active branch of the WARS in the ASE (Gohl *et al.* 2013a,b).

Following the recent hypothesis of Kipf *et al.* (2013) we infer that the magmatic bulge at the Moho discontinuity was the result of a long-distance magma flow which reached the Moho, grew continuously and then spilled over (Fig. 11). This magma bulge is likely to be responsible for the Outer Low in the BA and the corresponding elevated top-of-basement which is identified in seismic data (Gohl *et al.* 2013b). It seems reasonable, that the accumulation of magmatic material at the Moho cause uplift of the overlying structures (Burov & Guillou-Frottier 2005).



**Figure 11.** (a) interpreted 2-D gravity model based on the seismic refraction profiles AWI-20060100 and AWI-20060200. The top-of-basement was mapped by using the seismic reflection profiles AWI-20060100, AWI-20060200 and AWI-20100119. The black arrows show the flow direction of the inferred continental insulation flow (Kipf *et al.* 2013) from beneath Marie Byrd Land to the Marie Byrd Seamount Province. The blue arrows represent extensional rifting. The slides (b) to (e) show schematically the tectono-magmatic development of the margin from breakup of New Zealand and West Antarctica to Oligocene. MBL, Marie Byrd Land; NZ, New Zealand.

## 7 CONCLUSION

Geophysical data from the ASE provide new insights into the lithospheric architecture and tectono-magmatic development of this continental margin. Two deep crustal seismic profiles image the crustal and upper mantle structure of parts of the continental rise, slope and shelf. A continuous rise-to-shelf 2-D gravity model supports and expands on the velocity–depth models and enables the interpretation

of a tectono-magmatic history for the ASE margin from its breakup with Zealandia to the present and indicating a margin-wide process of magmatic underplating. The main findings are summarized as follows:

1. The geophysical data image the upper and lower crust and reveal a high-velocity layer at the base of the lower crust beneath the shelf. The crust is 10–14 km thick at the continental rise and up

to 29 km thick beneath the inner shelf. Seismic refraction data reveal *P*-wave velocities between 7.1 and 7.6 km s<sup>-1</sup> in the high-velocity layer indicating a margin-wide process of magmatic underplating whose thickness varies up to a maximum 10 km.

2. 2-D gravity modelling supports the hypothesis of a magmatic layer beneath the shelf and is consistent with the velocity–depth model. Indications of seaward-dipping reflectors in the seismic data suggest that breakup between greater New Zealand and West Antarctica may have been accompanied by magmatism not necessarily related to initial break-up.

3. Following the interpretation of Kipf *et al.* (2013), the high-velocity layer can be related to the Marie Byrd Seamount Province as product of a continental insulation flow which transported mantle material from beneath West Antarctica to the present-day Marie Byrd Seamount Province. The onset of the magma flow in the Palaeocene, which is maybe mantle originated, correlates with a major plate reorganization in the South Pacific (Cande *et al.* 2000). Magma accumulation at the base of the crust seems to be responsible for the elevated basement beneath the outer shelf of the Amundsen Sea Embayment. The absence of a gradational transition between the velocity body, normal upper crustal seismic velocities and a significant higher density of the observed HVL suggest that serpentinized mantle not is present beneath the ASE.

4. The crustal architecture, sedimentary setting and potential field data from the ASE indicate its formation during crustal extension. The constant crustal thickness and horst and graben structures suggest that this process was an expression of wide-mode rifting. Geophysical data show early stage, fully developed and failed initial rifting structures within the ASE suggesting a late active branch or integrated feature of the West Antarctic Rift System.

## ACKNOWLEDGEMENTS

We are grateful to the master, crews and scientific teams of the *RV Polarstern* expeditions ANT-XXIII/4 (2006) und ANT-XXVI/3 (2010) for their support in collecting new geophysical data from the ASE. This project was funded by the Deutsche Forschungsgemeinschaft (DFG) under project number GO 724/13–1 and is affiliated with Work Package 3.2 of the AWI research program PACES.

## REFERENCES

Anderson Don, L., 1989. *Theory of the Earth*, Blackwell Scientific Publications, <http://resolver.caltech.edu/CaltechBOOK:1989.001>.

Barton, P., 1986. The relationship between seismic velocity and density of continental crust – a useful constraint? *Geophys. J. R. astr. Soc.*, **87**, 195–208.

Bingham, R.G., Ferraccioli, F., King, E.C., Larter, R.D., Pritchard, H.D., Smith, A.M. & Vaughan, D.G., 2012. Inland thinning of West Antarctic Ice Sheet steered along subglacial rifts, *Nature*, **487**, 468–471.

Boillot, G. & Winterer, E.L., 1988. Drilling on the Galicia Margin: retrospect and prospect, in *Proceedings of the Ocean Drilling Program, Scientific Results*, Vol. 103, pp. 809–828, eds Boillot, G. & Winterer, E.L. Ocean Drilling Program, College Station.

Boillot, G., Beslier, M-O. & Comas, M., 1992. Seismic image of undercrusted serpentinite beneath a rifted margin, *Terra Nova*, **4**, 25–33.

Bradshaw, J.D., 1991. Cretaceous dispersion of Gondwana: continental and oceanic spreading in the south-west Pacific-Antarctic sector, in *Geological Evolution of Antarctica*, pp. 581–585, eds Thompson, M.R.A., Crame, J.A. & Thompson, J.W., Cambridge Univ. Press.

Buck, W.R., 1991. Modes of continental lithospheric extension, *J. geophys. Res.*, **96**, 20 161–20 178.

Burov, E. & Guillou-Frottier, L., 2005. The plume head-continental lithosphere interaction using a tectonically realistic formulation for the lithosphere, *Geophys. J. Int.* **161**, 469–490.

Cande, S.C., Stock, J.M., Müller, R.D. & Ishihara, T., 2000. Cenozoic motion between East and West Antarctica, *Nature*, **404**, 145–150.

Carlson, R.L. & Miller, D.J., 2003. Mantle wedge water contents estimated from seismic velocities in partially serpentinized peridotites, *Geophys. Res. Lett.*, **30**(5), doi:10.1029/2002GL016600.

Chian, D., Loudon, K.E., Minshull, T.A. & Whitmarsh, R.B., 1999. Deep structure of the ocean-continent transition in the southern Iberia Abyssal Plain from seismic refraction profiles: ocean Drilling Program (Legs 149 and 173) transect, *J. geophys. Res.*, **104**, 7443–7462.

Christensen, N.I. & Mooney, W.D., 1995. Seismic velocity structure and composition of the continental crust. A global view, *J. geophys. Res.*, **100**, 9761–9788.

Christensen, N.I., 1996. Poisson's ratio and crustal seismology, *J. geophys. Res.*, **101**, 3139–3156.

Cianciara, B. & Marcak, H., 1976. Interpretation of gravity anomalies by means of local power spectra, *Geophys. Prosp.*, **24**, 273–286.

Dalziel, I.W.D. & Elliot, D.H., 1982. West Antarctica: problem child of Gondwanaland, *Tectonics*, **1**, 3–19.

Davey, F.J. & De Santis, L., 2006. A multi-phase rifting model for the Victoria Land Basin, Western Ross Sea, *Antarctica*, 303–308.

Davy, B. & Wood, R.A., 1994. Gravity and magnetic modelling of the Hikurangi Plateau, *Mar. Geol.*, **118**, 139–151.

Eagles, G., Gohl, K. & Larter, R.D., 2004a. High-resolution animated tectonic reconstruction of the South Pacific and West Antarctic margin, *Geochem., Geophys., Geosyst.*, **5**, doi:10.1029/2003GC000657.

Eagles, G., Gohl, K. & Larter, R., 2004b. Life of the Bellingshausen plate, *Geophys. Res. Lett.*, **31**, doi:10.1029/2003GL019127.

Ebinger, C., Deino, J.A., Drake, R.E., Tesha, A.L., Kronenberg, A. & Tullis, F., 1989. Chronology of volcanism and rift basin propagation: Rungwe volcanic province, East Africa, *J. geophys. Res.*, **94**, 15 785–15 803.

Gohl, K., 2012. Basement control on past ice sheet dynamics in the Amundsen Sea Embayment, West Antarctica, *Palaeogeog. Palaeoclimat. Palaeoecol.*, **335–336**, 35–41.

Gohl, K. *et al.*, 2007. Geophysical survey reveals tectonic structures in the Amundsen Sea embayment, West Antarctica, in *Proceedings of the 10th Int. Symposium of Antarctic Earth Sciences*, eds Cooper, A.K. & Raymond, C.R., USGS Open-File Report 2007–1047, doi:10.3133/of2007–1047.srp047.

Gohl, K., Denk, A., Eagles, G. & Wobbe, F., 2013a. Deciphering tectonic phases of the Amundsen Sea Embayment shelf, West Antarctica from a magnetic anomaly grid, *Tectonophysics*, **585**, 113–123.

Gohl, K. *et al.*, 2013b. Seismic stratigraphic record of the Amundsen Sea Embayment shelf from pre-glacial to recent times: evidence for a dynamic West Antarctic ice sheet, *Mar. Geol.*, **344**, 115–131.

Götze, H.J. & Lahmeyer, B., 1988. Application of three-dimensional interactive modelling In gravity and magnetics, *Geophysics* **53**(8), 1096–1108.

Grobys, J.W.G., Gohl, K. & Eagles, G., 2008. Quantitative tectonic reconstructions of Zealandia based on crustal thickness estimates, *Geochem., Geophys., Geosyst.*, **9**(1), Q01005, doi:10.1029/2007GC001691.

Grobys, J.W.G., Gohl, K., Uenzelmann-Neben, G. & Barker, 2009. Extensional and Magmatic nature of the Campbell Plateau and Great South Basin from deep crustal studies, *Tectonophysics*, **472**, 213–225.

Grunow, A.M., Kent, D.V. & Dalziel, I.W.D., 1991. New paleomagnetic data from Thurston Island: implications for the tectonics of West Antarctica and Weddell Sea opening, *J. geophys. Res.*, **96**(B11) 17 935–17 954.

Hopper, J., Dahl-Jensen, T., Holbrook, W., Larsen, H., Lizarralde, D., Korenaga, J., Kent, G. & Kelemen, P., 2003. Structure of the SE Greenland margin from seismic reflection and refraction data: implications for nascent spreading center subsidence and asymmetric crustal accretion during North Atlantic opening, *J. geophys. Res.*, **108**, B5, doi:10.1029/2002JB001996.

Hamilton, W., 1987. Crustal extension in the Basin and Range Province, south-western United States, in *Continental Extensional Tectonics*, Vol. 28, pp. 155–176, eds Coward, M.P., Dewey, J.F. & Hancock, P.L., Geological Society Special Publications.

- Jordan, T.A., Ferraccioli, F., Vaughan, D.G., Holt, J.W., Corr, H., Blankenship, D.D. & Diehl, T.M., 2010. Aerogravity evidence for major crustal thinning under the Pine Island Glacier region (West Antarctica), *Bull. geol. Soc. Am.*, **122**, 714–726.
- Karner, G.D. & Watts, A.B., 1983. Gravity anomalies and flexure of the lithosphere at mountain ranges, *J. geophys. Res.*, **88**, 10 449–10 477.
- Kipf, A., Mortimer, N., Werner, R., Gohl, K., van den Bogaard, P., Hauff, F. & Hoernle, K. (2012). Granitoids and dykes of the Pine Island Bay region, West Antarctica, *Antarctic Sci.*, **24**(5), 473–484.
- Kipf, A., Hauff, F., Werner, R., Gohl, K., van den Bogaard, P., Hoernle, K., Maicher, D. & Klügel, A., 2013. Seamounts off the West Antarctic margin: a case of non-hotspot intraplate volcanism, *Gondwana Res.*, doi:10.1016/j.gr.2013.06.013.
- Larter, R.D., Cunningham, A.P., Barker, P.F., Gohl, K. & Nitsche, F.O., 2002. Tectonic evolution of the Pacific margin of Antarctica—1. Late Cretaceous tectonic reconstructions, *J. geophys. Res.*, **107**(B12), 2345, doi:10.1029/2000JB000052.
- Lindow, J., Spiegel, C., Johnson, J., Lisker, F. & Gohl, K., 2011. Constraining the latest stage exhumation of Marie Byrd and Ellsworth Land, West Antarctica, in *Proceedings of the 11th International Symposium on Antarctic Earth Science*, Edinburgh, Scotland.
- Llubes, M., Florsch, N., Legresy, B., Lemoine, J., Loyer, S., Crossly, D. & Remy, F. 2003. Crustal thickness in Antarctica from CHAMP gravimetry, *Earth planet. Sci. Lett.*, **212**, 103–117.
- Luyendyk, B., Wilson, D.S. & Siddoway, C.S., 2003. Eastern margin of the Ross Sea Rift in western Marie Byrd Land, Antarctic: crustal structure and tectonic development, *Geochem., Geophys., Geosyst.* **4**, doi:10.1029/2002GC000462.
- Malahoff, A., Kolotyckina, I.Y., Midson, B.P. & Massoth, G.I., 2006. A decade of exploring a submarine intraplate volcano: hydrothermal manganese and iron at Lo’ihi volcano, *Geochem., Geophys., Geosyst.*, **7**, 1525–2027.
- Mayes, C.L., Lawver, L.A. & Sandwell, D.T., 1990. Tectonic history and new isochron chart of the South Pacific, *J. geophys. Res.*, **95**, 8543–8567.
- McAdoo, D.C. & Laxon, D., 1997. Antarctic tectonics: constraints from an ERS-1 satellite marine gravity field, *Science*, **276**, 556–560.
- Minshull, T., 2009. Geophysical characterisation of ocean-continent transition at magma-poor rifted margins, *C. R. Geosci.*, **341**, 382–393.
- Mjelde, R., Kasahara, J., Shimamura, H., Kamimura, A., Kanazawa, T., Kodaira, S. & Shiobara, T., 2002. Lower crustal seismic velocity-anomalies; magmatic underplating or serpentinized peridotite? Evidence from the Voring Margin, NE Atlantic, *Mar. geophys. Res.*, **23**, 169–183.
- Mortimer, N., Hoernle, K., Hauff, F., Palin, J.M., Dunlap, W.J., Werner, R. & Faure, K., 2006. New constraints on the age and evolution of the Wishbone Ridge, southwest Pacific Cretaceous microplates, and Zealandia–West Antarctica breakup, *Geology* **34**, 185–188.
- Mukasa, S.B. & Dalziel, I.W.D., 2000. Marie Byrd Land, West Antarctica: evolution of the Gondwana’s Pacific margin constrained by zircon U–Pb geochronology and feldspar common-Pb isotopic compositions. *Bull. geol. Soc. Am.*, **112**, 611–627.
- Mutter, J.C., Talwani, M. & Stoffa, P.L., 1984. Evidence for a thick oceanic crust off Norway, *J. geophys. Res.*, **89**, 483–502.
- Nafe, J.E. & Drake, C.L., 1963. Physical properties of marine sediments, in *The Sea*, Vol. **3**, pp. 794–815, ed. Hill, M.N., Interscience.
- Nitsche, F.O., Jacobs, S., Larter, R.D. & Gohl, K., 2007. Bathymetry of the Amundsen Sea Continental Shelf: implications for geology, oceanography, and glaciology, *Geochem., Geophys., Geosyst.*, **8**, Q10009, doi:10.1029/2007GC001694.
- Reid, I., 1994. Crustal structure of a non-volcanic rifted margin east of Newfoundland, *J. geophys. Res.*, **99**, 161–180.
- Rocchi, S., LeMasurier, W.E. & Di Vincenzo, G., 2006. Oligocene to Holocene erosion and glacial history in MBL, West Antarctica, inferred from exhumation of the Dorrel Rock intrusive complex and from volcano morphologies, *Geol. Soc. Am. Bull.* **118**, 991–1005.
- Rosenbaum, G., Lister, G.S. & Duboz, C., 2002. Relative motions of Africa, Iberia and Europe during Alpine orogeny, *Tectonophysics*, **359**, 117–129.
- Schubert, G., Trucotte, D.L. & Olsen, P., 2001. *Mantle Convection in the Earth and Planets*, 1st edn, Cambridge Univ. Press.
- Siddoway, C., 2008. Tectonics of the West Antarctic rift system: new light on the history and dynamics of distributed intracontinental extension. Antarctica: a keystone in a Changing World, in *Proceedings of the 10th International Symposium on Antarctic Earth Sciences*, The National Academies Press, Washington, DC, pp. 91–114.
- Smith, A.M., Jordan, T.A., Ferraccioli, F. & Bingham, R.G., 2013. Influence of subglacial conditions on ice stream dynamics: seismic and potential field data from Pine Island Glacier, West Antarctica, *J. geophys. Res.*, **118**(4), 1471–1482.
- Spector, A. & Grant, F.S., 1970. Statistical models for interpreting aeromagnetic data, *Geophysics*, **35**, 293–302.
- Storey, B.C., 1991. The crustal blocks of West Antarctica within Gondwana: Reconstruction and breakup model, in *Geological Evolution of Antarctica*, pp. 587–592, eds. Thompson, M.R.A., Crame, J.A. & Thompson, J.W., Cambridge University Press.
- Torge, W., 1989. *Gravimetry*, Walter de Gruyter, pp. 465.
- Voss, M. & Jokat, W., 2007. Continent-ocean transition and voluminous magmatic underplating derived from *P*-wave velocity modelling of the Greenland continental margin, *Geophys. J. Int.*, **170**, 580–604.
- Watts, A.B. & Fairhead, J.D., 1999. A process-oriented approach to modelling the gravity signature of continental margins, *Leading Edge*, **18**(2), 258–263.
- Whitmarsh, R.B., White, R.S., Horsefield, S.J., Sibuet, J., Recq, M. & Louvel, V., 1996. The ocean-continent boundary off the western continental margin of Iberia: crustal’s structure west of Galician Bank, *J. geophys. Res.*, **101**, 291–314.
- Winberry, J.P. & Anandakrishnan, S., 2004. Crustal structure of the West Antarctic rift system and Marie Byrd Land hotspot, *Geology*, **32**(11), 977–980.
- Wobbe, F., Gohl, K., Chambord, A. & Sutherland, R., 2012. Structure and break-up history of the rifted margin of West Antarctica in relation to Cretaceous separation from Zealandia and Bellinghousen plate motion, *Geochem., Geophys., Geosyst.*, **13**, Q04W12, doi:10.1029/2011GC003742.
- Zelt, C.A. & Smith, R.B., 1992. Seismic traveltime inversion for 2-D crustal velocity structure, *Geophys. J. Int.*, **108**(1), 16–34.